

## RESEARCH ARTICLE OPEN ACCESS

# Thermokarst Lagoons: Distribution, Classification and Dynamics in Permafrost-to-Marine Transitions

Maren Jenrich<sup>1,2</sup>  | Maria Prodingler<sup>1,3</sup> | Ingmar Nitze<sup>1</sup> | Guido Grosse<sup>1,2</sup> | Jens Strauss<sup>1</sup> 

<sup>1</sup>Permafrost Research Section, Alfred Wegener Institute Helmholtz Centre for Polar and Marine Research, Potsdam, Germany | <sup>2</sup>Institute of Geosciences, University of Potsdam, Potsdam, Germany | <sup>3</sup>Institute of Geography, Universität Hamburg, Hamburg, Germany

**Correspondence:** Maren Jenrich ([maren.jenrich@awi.de](mailto:maren.jenrich@awi.de))

**Received:** 9 April 2025 | **Revised:** 9 April 2025 | **Accepted:** 10 June 2025

**Funding:** M.J. was funded by the Deutsche Bundesstiftung Umwelt (project ‘Characterization of Organic Carbon and Assessment of Greenhouse Gas Emissions in a Warming Arctic’; AZ 20020/676). I.N. and G.G. were funded by German Federal Ministry for Economic Affairs and Climate Action (BMWK) research project ML4EARTH as well as National Science Foundation (NSF) and [google.org](https://www.google.org) ‘Permafrost Discovery Gateway’ (NSF Opp: 1927872 and 2052107). The Alfred Wegener Institute Helmholtz Centre for Polar and Marine Research supported field research with base funding and provided funds for open access publication.

**Keywords:** Arctic coastal dynamics | Arctic lagoons | area change analysis | lagoon classification | permafrost | thermokarst

## ABSTRACT

The transition of permafrost landscapes to marine environments, driven by climate change, plays a crucial role in the global carbon cycle. Thermokarst lagoons, formed along permafrost coasts when thermokarst lakes get connected to the sea, are key features in this transition. Using remote sensing imagery, we manually mapped and classified 520 thermokarst lagoons along the coastline of five Arctic shelf seas (Laptev, East Siberian, Chukchi, Alaskan Beaufort and Canadian Beaufort seas) between the Taymyr and Tuktoyaktuk peninsulas, and most were located along the Canadian Beaufort Sea. These lagoons cover a total area of 3457 km<sup>2</sup>, with strong regional variations in both size and distribution. Based on their sea connectivity, we categorised the lagoons into five classes, with 55% in early transition stages (very low to low connected). From 2000 to 2021, lagoon area increased in all regions, with the Alaska Beaufort Sea coast showing the most growth (+1.34%). Smaller and isolated lagoons expanded faster than those in lagoon systems or deltas. Our analysis links thermokarst lagoon distribution to coastal erosion, land cover, ground ice and organic carbon, showing that most lagoons are located in areas of thermokarst lake coverage and high coastal erosion. This unique pan-Arctic dataset serves as a foundation for understanding thermokarst lagoon dynamics and their role in the rapidly changing Arctic environment.

## 1 | Introduction

The transition of permafrost landscapes to marine environments due to climate change is a critical process with significant implications for the global carbon cycle [1–4]. Permafrost holds a vast amount of organic carbon (~1460–1600 GT; [5–7]), and permafrost thaw leads to the partial mobilisation and degradation of this previously sequestered organic carbon, potentially creating a feedback loop that exacerbates climate change [8, 9].

Especially vulnerable are deposits including excess ice, which are prone to surface subsidence and also high coastal erosion rates [10, 11]. Understanding the dynamics of these transitions is important for predicting future climate scenarios and mitigating their impacts. Both permafrost coastal erosion and inundation of low-lying areas are important processes that result in terrestrial permafrost transitioning to a marine environment. In the Arctic, lagoons are providing a unique setting where these types of transitions and their consequences can be studied in detail.

M.J. and M.P. contributed equally to this work.

This is an open access article under the terms of the [Creative Commons Attribution](https://creativecommons.org/licenses/by/4.0/) License, which permits use, distribution and reproduction in any medium, provided the original work is properly cited.

© 2025 The Author(s). *Permafrost and Periglacial Processes* published by John Wiley & Sons Ltd.

Arctic lagoons are critical habitats that support diverse and highly productive ecosystems, playing a key role in the structure and functioning of the Arctic coastal environment [12, 13]. These shallow, semi-enclosed water bodies act as ecological buffers between terrestrial and marine environments, providing crucial habitats for a wide variety of species, including migratory birds, fish and marine mammals [12–15]. For example, in Alaska, the Beaufort Lagoon LTER (Long Term Ecological Research) programme has emphasised the importance of these ecosystems, highlighting their sensitivity to changes in freshwater input, sea ice dynamics and coastal erosion [16, 17]. Studies show that more sheltered lagoons foster greater biodiversity, whereas less protected lagoons exhibit lower diversity of trophic niches among fish populations [18]. Research from Siberia and Canada highlighted the role of lagoons in shaping coastal geomorphology and influencing sediment fluxes, nutrient cycling, carbon storage and their complex hydrochemistry [19–21]. Across Alaska, Canada and Russia, studies consistently show that lagoons may serve as hotspots of biological activity, supporting both local biodiversity and subsistence practices of Indigenous communities (e.g., [22]).

Unlike barrier-island lagoons, which develop when spits or sandbars enclose a water body, thermokarst lagoons form exclusively in Arctic thermokarst coastal lowland environments when thermokarst lakes or basins are inundated by the sea (Figure 1). These lagoons have distinct geomorphological features, including a round to oval shape and well-defined shorelines distinguishing them from other coastal lagoons. They

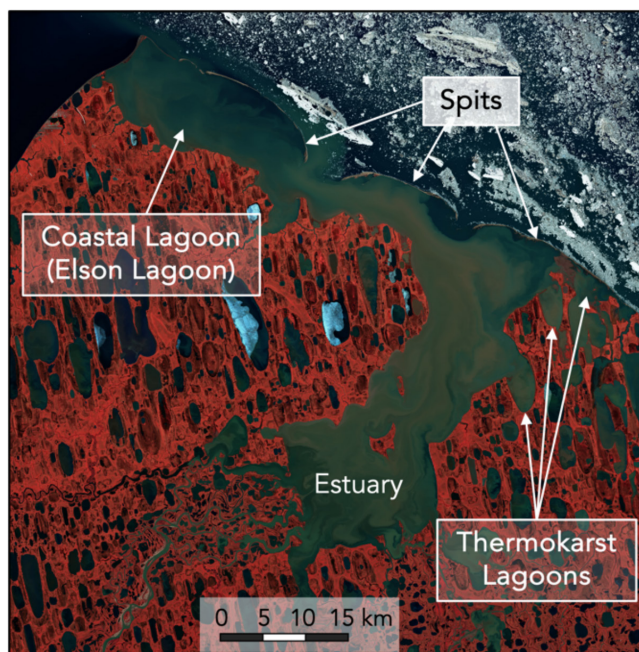


**FIGURE 1** | Sentinel-2 satellite image of northern Alaska showcasing different coastal water body types along a typical Arctic lowland coastline. Thermokarst lagoons, formed from inundated thermokarst lakes and drained lake basins, are distinct from the larger, barrier island-separated coastal lagoon (here, Elson Lagoon) and a wide river estuary. *Source:* ESA, false-colour Sentinel 2 image from 2024-07-11. [Colour figure can be viewed at [wileyonlinelibrary.com](https://onlinelibrary.wiley.com)]

maintain at least intermittent connections to the sea through inlets or visible channels formed after thermokarst lake drainage or regular water exchanges driven by tides or storm surges [23, 24]. Thermokarst lagoon formation is driven by coastal erosion, sea-level rise and permafrost thaw-induced ground subsidence [25]. Previous thermokarst lagoon research focused, for example, on coastline evolution and drowning of thermokarst-affected landscapes [20, 26, 27] or lagoon sediment characteristics [21, 28–31]. We here develop a broader generalisation scheme for thermokarst lagoons and a pan-Arctic assessment of their distribution and classification, because they are key features in the permafrost-to-marine transition and a generalised scheme will help better understanding of thermokarst lagoon development and the environmental settings.

Previous research has laid the groundwork for categorising Arctic lagoons based on their connectivity to the marine environment [22]. The classification of Arctic lagoons into ‘barrier island’, ‘stable connection’, ‘intermittent connection’ and ‘closed’ on a gradient from high to low connectivity is comparable to the initial thermokarst lagoon classification by Jenrich et al. [30], though Fraley et al. [22] focused on coastal lagoons without taking thermokarst processes into account. Specifically for thermokarst lagoons, the initial classification system by Jenrich et al. [30] categorised lagoons into ‘open’, ‘semi-closed’ and ‘nearly closed’ systems based on their connectivity and coastal erosion gradients. Angelopoulos et al. [23] provided a first distribution map, and the first total area estimation was conducted by Jenrich et al. [30], followed by an extensive pan-Arctic lagoon area estimation by Yang et al. [32]. This research showed that thermokarst lagoons occupy approximately 2579 km<sup>2</sup>, an area roughly equivalent to the country of Luxembourg.

Despite these advances, several knowledge gaps remain. In particular, lagoon connectivity is an important parameter that determines water exchange, hydrochemistry and biogeochemistry, as well as ecological exchange [33, 34]. Connectivity might be affected by spatial constraints such as channel length and depth or by temporal constraints, for example, due to seasonal ice formation that restricts or seals connecting channels [35]. Hence, the subdivision of interconnected lagoon systems into individual lagoons needs more precision, also impacting the accurate estimation of their number and area. The existing classification system remains insufficient for the detailed categorisation required for complex or nested lagoon systems. Moreover, the biogeochemical and hydrochemical diversity within these systems, influenced by differences in connectivity, sediment input and salinity, needs a more refined classification approach. Furthermore, although thermokarst lagoon area change has not yet been studied, it is conceivable that the nature of lagoons, that is, the openness or closedness of their connection, could impact erosion of their shorelines because it impacts salinity, water temperatures and wave and current dynamics, all of which are factors known to affect coastal erosion. Some of the most prominent changes in permafrost-affected areas are due to coastal erosion [36–38] and widespread thermokarst lake changes [39, 40]. Although those have been widely studied using remote sensing techniques, research concerning area change dynamics of thermokarst lagoons is lacking.

This paper addresses these abovementioned gaps by aiming to provide a unique dataset that includes the count, area and classification of thermokarst lagoons on a pan-Arctic scale and further the change in lagoon area over 20 years. By employing manual mapping techniques and an improved classification system, this study aims to offer a comprehensive understanding of thermokarst lagoon dynamics and their role in the permafrost-to-marine transition.

## 2 | Methods

Thermokarst lagoons were differentiated from other types of lagoons based on their high roundness that suggest an origin as thermokarst lake or basin, their presence along a lowland coast dominated by thermokarst lake and basin systems and the absence of wide spits and barrier islands enclosing a coastal water body, which is typical for other coastal lagoon types.

### 2.1 | Improved Lagoon Mapping Approach

Building on previous mapping efforts [23, 24], we refined the classification of thermokarst lagoons by distinguishing interconnected sub-lagoons as individual entities where the original basin shape was still recognisable. This distinction acknowledges differences in geomorphological legacy, hydrochemistry, biogeochemistry and sedimentology among sub-lagoons.

A water body was classified as a thermokarst lagoon if it met the following criteria:

1. Located in a thermokarst environment;
2. Round to oval-shaped depression with a discernible shoreline;
3. Minimum of 500 m in diameter;
4. At least intermittent connection with the sea either through:
  - a. a visible channel with a maximum length of 1 km;
  - b. separation only by a narrow beach;
  - c. or a maximum elevation difference to the sea of  $\leq 1.5$  m, which ensures regular water exchange via spring tides or storm surges.

Differences in altitude between land and sea were determined using the ArcticDEM digital elevation model and hillshade [41] in combination with ESA Sentinel-2 false-colour satellite imagery. A median image composite from August and September 2018 with a spatial resolution of 10 m served as the base imagery.

The methodological approach of the mapping and the datasets used are shown in Figure 2. Mapping was conducted in QGIS Version 3.34 using Sentinel-2 imagery accessed via the Copernicus Browser (Copernicus Sentinel data). Images were selected with a cloud cover of less than 30% from 2023-07-01 to 2023-08-30, utilising true-colour (B4: red, B3: green, B2: blue) and false-colour composites (B8: NIR, B4: red, B3: green) to

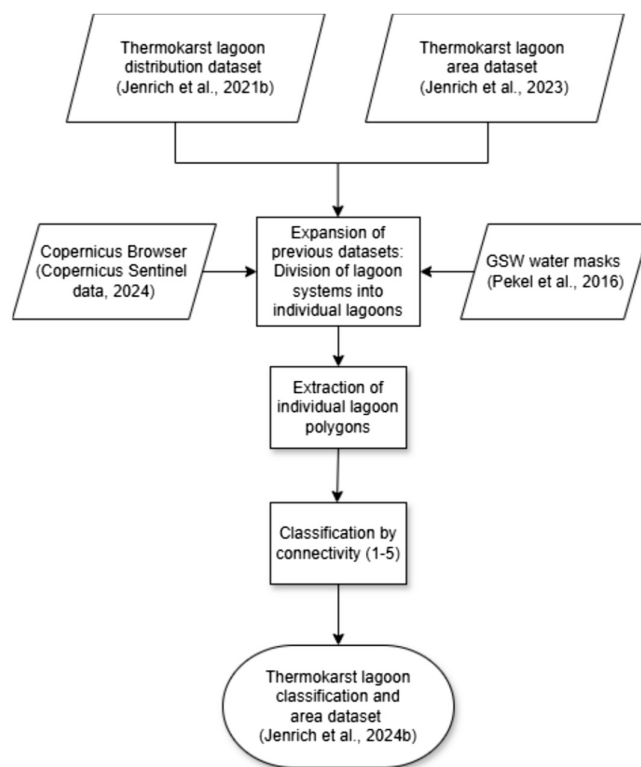


**FIGURE 2** | Flow chart depicting the datasets (parallelogram) that contributed to this study, the main methodological steps (boxes) of the lagoon mapping and the dataset that the study is based on (oval). Datasets: [42–46].

enhance visibility of natural boundaries. Features such as sand spits, sandbanks and shoals were used as visual references for delineation. Additional imagery basemaps, including Google Satellite layer and ESRI Satellite/ArcGIS World Imagery (Esri, Maxar, Earthstar Geographics and the GIS User Community), provided supplementary context but were secondary due to unclear acquisition dates.

Water masks for sub-lagoon delineation were derived from the Global Surface Water (GSW) dataset [46], which utilises Landsat-5, Landsat-7 and Landsat-8 data from 1984 to 2021 at 30 m resolution. These masks were generated in Google Earth Engine [47] based on the occurrence dataset from GSW in Version 1.4 [46] using a threshold of  $> 75\%$ . The resulting raster images were vectorised in QGIS to guide lagoon mapping. The basin shapes from the water masks provided crucial reference points for accurate boundary determination based on lagoon polygons (Figure 3).

Pre-existing thermokarst lagoon boundaries from Jenrich et al. [44] were integrated and refined where necessary. Adjustments were made in cases where the original mapping did not align with expected lagoon morphology, leading to slight variations in area size. For example, in *Tesh 15 (ABS\_010)*, the current study mapped the lagoon based solely on its distinct round shape, whereas Jenrich et al. [44] included an elongated, estuary-like outlet. This refinement led to improved accuracy in lagoon size estimation.



**FIGURE 3** | Exemplary lagoon extraction for individual lagoons (blue circles) and connected lagoons in lagoon systems (white circles) at the Northern Head of the Mackenzie Delta, Richards Island, Canadian Beaufort Sea. CBS 213 and CBS 214 are examples of newly formed lagoons that have been shrinking in recent years due to drainage. Water mask is based on the Global Surface Water dataset (Pekel et al. 2016), and coalesced water bodies have been split with a straight by line at the narrowest part between visually identifiable sub-basins. *Source*: True-colour Sentinel-2 satellite image from 2023-08-26. [Colour figure can be viewed at [wileyonlinelibrary.com](https://onlinelibrary.wiley.com)]

Water mask datasets in Jenrich et al. [44] were based on data spanning from 1984 to 2018, whereas this study incorporated an updated range of 1984–2021. The resulting difference in total lagoon area was  $0.33\% \pm 0.94\%$  (median: 0.04%), also pointing at the dynamic nature of Arctic coastal water surfaces. The use of an updated dataset has increased the precision of area calculations.

By implementing these refinements and developing clear criteria for manual mapping, this study ensures a more consistent and accurate assessment of thermokarst lagoon distribution and area in permafrost regions.

To define lagoon boundaries and create distinct polygons, the ‘split with lines’ function in QGIS was used. This step was particularly crucial in complex landscapes like the Lena Delta, where a Sentinel-2 RGB composite (acquisition date 2023-06-08) provided additional clarity. Lagoon boundaries were delineated based on:

1. Water masks: Boundaries were set at the narrowest points of lagoon openings, as derived from the GSW dataset.

2. Satellite imagery: Sentinel-2 imagery allowed identification and tracking of natural morphological features such as sandbanks, barriers and shoals.

To ensure consistency in area calculations, we used the EPSG:3413 coordinate reference system (WGS 84/NSIDC Sea Ice Polar Stereographic North), avoiding discrepancies from re-projection into UTM Zones. This approach differs from Jenrich [24], where UTM-based calculations were used.

## 2.2 | Classification

The 520 mapped thermokarst lagoons were then classified manually into five distinct classes based on their connectivity to the sea (Table 1) using a geomorphological approach that did not account for bathymetry.

This classification reflects different stages of the lake-to-sea transition and considers the presence of natural barriers such as sand banks and spits, the length of a channel or width of a lagoon opening and the distance from the sea. Exemplary ranges from lagoons of each class are presented in Table 1. A table with additional examples can be found in Table S1.

**Class 1:** This class is characterised by lagoons with very low connectivity to the sea. Exchange is strongly limited by a long and/or narrow channel. These lagoons may exhibit temporary lake characteristics and represent the least advanced stage in the lake-to-sea transition. In some cases, they are subsequent lagoons with very limited exchange due to the restrictive nature of the channel and/or the high distance to the sea.

**Class 2:** Lagoons in this class have low connectivity, with exchange limited by a very small opening or narrow channel. These may be subsequent lagoons with less connection to the primary lagoon, either due to the small channel size or high distance from the sea.

**Class 3:** This class represents lagoons with medium connectivity. Exchange is limited either temporally or spatially by larger barrier islands or sand spits compared to Class 4. These lagoons can also be subsequent lagoons that are well connected to the previous lagoon.

**Class 4:** Lagoons classified as Class 4 exhibit high connectivity to the sea. Exchange is only slightly limited by the presence of barrier islands or sand spits that constrict the inlet slightly. This class also includes subsequent lagoons that are very well connected to the previous lagoon, with minimal obstruction to seawater exchange.

**Class 5:** Representing the most advanced stage in the lake-to-sea transition, Class 5 lagoons have very high connectivity to the sea. The inlet is not limited by sand banks or spits, allowing for unrestricted exchange with the sea.

This classification framework allows for a detailed understanding of the connectivity levels of thermokarst lagoons and their respective stages in the transition from lake to marine environments and works for single lagoons as well as for lagoon systems.

**TABLE 1** | Thermokarst lagoon classification by connectivity to the sea, based on a geomorphological approach. The classes increase with the growing openness of the lagoon and the stronger connection to the sea. Characteristics of classes are CL (channel length), W (width of channel/lagoon opening), D (distance to open sea) and B (coastal barriers like beaches or spits). Examples of the classification are provided in the satellite image of the eastern tip of Tuktoyaktuk Peninsula, NWT, Canada.

Class	Connectivity	Openness	Characteristics	Examples
1	Very low	Nearly closed	CL: 430–1000 m W: 70–2000 m D: 15–19,000 m B: < 100 m in width if no channel present or none	
2	Low	Limited open	CL: 150–1000 m W: 40–2000 m D: 0–12,000 m B: Leaky or none	
3	Medium	Semi-open	CL: No channel W: 80–2600 m D: 0–4500 m B: With wide openings or none	
4	High	Mostly open	CL: No channel W: 420–5000 m D: 0–7000 m B: Almost absent or none	
5	Very high	Always open	CL: No channel W: 500–2700 m D: 0–1500 m B: None	

Source: False-colour Sentinel 2 image from 2023-08-05.

## 2.3 | Lagoon Area Change

### 2.3.1 | Water Area Extraction

In order to explore thermokarst lagoon area changes on a larger scale, the GSW dataset [46] and its annual data availability were used. Area information for individual years from 2000 through 2021 was extracted through Google Earth Engine using the existing lagoon polygons. We extracted all four layers of the GSW data, including permanent and seasonal water area, as well as land and no data area for debugging and data filtering with values in square kilometres (km<sup>2</sup>) per lagoon for each year. We refrained from using data before 2000 due to highly limited data availability, particularly over Siberia.

### 2.3.2 | Data Cleaning

The extracted annual surface water data for each lagoon required pre-processing before data analysis. Many lagoons contained NoData pixels in the original surface water dataset due to missing data, primarily resulting from lower acquisition frequencies before 2013 prior to the launch of Landsat-8, limited downlink capacities of Landsat and challenging acquisition conditions for optical satellite data in Arctic coastal regions [48–50].

To ensure complete surface water information, we flagged and removed data points for each year and lagoon with a NoData

fraction exceeding 2%. After this clean-up, the fraction of lagoons with NoData ranged from 1.0% in 2019 to 87.4% in 2003, with a notably higher fraction of missing data before 2013 (see Figure S3).

Subsequently, we merged the permanent and seasonal water classes into a single water class. For further time-series analysis, we implemented data imputation strategies to fill the gaps. Assuming that lagoon areas are comparably stable with minimal interannual variation and that the remaining data points are of good quality, we first applied linear interpolation to fill gaps based on local linear functions of the nearest data points in time. For NoData at the edges of the time series, we used forward- and backward-filling techniques, taking the nearest data point before or after the gap, respectively. As a result, we obtained a complete annual surface water area time series for all lagoons from 2000 to 2021.

### 2.3.3 | Data Aggregation and Change Analysis

We calculated the linear trends of area for each lagoon using ordinary least-squares regression over the entire period, which included the slope, intercept, *p* value and *r*<sup>2</sup>. Next, we aggregated the results by region, class and lagoon type to identify commonalities and differences in lagoon connectivity.

For the grouped statistics, we summarised the mean area per year. Additionally, we computed the mean normalised

change, which represents the average percentage change for individual lagoons from 2000 to 2021, as well as the overall normalised change, reflecting the total change within each region or class.

### 2.3.4 | Statistical Analyses

We assessed the statistical significance of lagoon area change rates (slope values) across regions and lagoon classes using a two-step approach. First, the Shapiro–Wilk test identified non-normal distributions in our samples, precluding the use of parametric *t*-tests. We therefore implemented non-parametric alternatives: the Kruskal–Wallis test for regional pairwise comparisons, which is practically the Mann–Whitney *U* test. Next, we compared single regions (adjacent seas) and lagoon classes against the total lagoon population using Wilcoxon signed-rank tests. All analyses were conducted in Python using SciPy’s statistical module (scipy.stats).

## 2.4 | Relationship Between Thermokarst Lagoon and Lake Area

We analysed the relationship between lagoon and lake area. Lakes were extracted from the Global Lakes and Wetlands

Database [51]. Lakes  $\geq 0.1 \text{ km}^2$  within a 30 km coastal buffer (ARCADE database; [52]) were included, without filtering for thermokarst characteristics. All lakes fell within continuous or discontinuous permafrost zones and were grouped by sea [53]. We visualised the size distribution using histograms with fixed bins of  $3 \text{ km}^2$  to ensure comparability.

Lakes and lagoons for each coast were categorised by size using quartiles: small ( $0.1 < 0.8 \text{ km}^2$ ), medium ( $0.8 < 1.2 \text{ km}^2$ ), large ( $1.2 < 2.4 \text{ km}^2$ ) and very large ( $\geq 2.4 \text{ km}^2$ ). Afterwards the difference between lake and lagoon quartiles was calculated, and the deviation (absolute values) further grouped in quartiles: small ( $1.2 < 11.1\%$ ), medium ( $11.1 < 21.0\%$ ), large ( $21.0 < 30.9\%$ ) and very large ( $\geq 30.9\%$ ).

## 3 | Results

### 3.1 | Distribution and Size of Thermokarst Lagoons

In total, we identified 520 thermokarst lagoons along the Arctic coast between the Taymyr Peninsula and Tuktoyaktuk Peninsula (Figure 4). Table 2 provides an overview of lagoon distribution across various Arctic coastal regions, lagoon types and lagoon classes. The Canadian Beaufort Sea has the highest



**FIGURE 4** | (a) Pan-Arctic permafrost map of the 520 thermokarst lagoons located along the Arctic coast between the Taymyr Peninsula (Siberia, Russia) and the Tuktoyaktuk Peninsula (Northwest Territories, Canada); number of lagoons in brackets. Detailed map of examples of thermokarst lagoons within lagoon systems located in the Lena Delta (b) and at the Northern Head of Richards Island, Mackenzie Delta, Canada (c). *Source:* A: service layer credits: Permafrost distribution: [53]; other layer: Natural Earth; B: Sentinel 2 image from 08.08.2023, natural colours; C: Sentinel 2 image from 16.08.2023 in natural colours. [Colour figure can be viewed at [wileyonlinelibrary.com](https://onlinelibrary.wiley.com)]

**TABLE 2** | Number, size and spatial distribution of thermokarst lagoons, classified by type and connectivity, along the Arctic coast from the Taymyr Peninsula (Siberia) to the Tuktoyaktuk Peninsula (Canada). The deviation between Delta and non-Delta lagoons is based on data published by Tessler et al. [54].

Category		Lagoon number	Lagoons distribution per category	Lagoon area km <sup>2</sup>	Mean lagoon area per category km <sup>2</sup>	Share of lagoon area category
<b>Total</b>		520	100%	3457	6.6	100%
Region	Canadian Beaufort Sea	243	47%	592	2.4	17%
	Alaska Beaufort Sea	70	13%	277	4.0	8%
	Chukchi Sea	57	11%	1362	23.9	39%
	East Siberian Sea	46	9%	353	7.7	10%
	Laptev Sea	104	20%	872	8.4	25%
Type	Delta <sup>a</sup>	152	29%	2712	17.8	78%
	Non-delta <sup>a</sup>	368	71%	744	2.0	22%
	Single lagoon	159	31%	675	4.2	20%
Connectivity class	Part of lagoon system	361	69%	2782	7.7	80%
	1	167	32%	792	4.7	23%
	2	119	23%	658	5.5	19%
	3	117	23%	989	8.5	29%
	4	74	14%	819	11.1	24%
	5	43	8%	199	4.6	6%

<sup>a</sup>Based on Tessler et al. [54].

lagoon count with 243, including 63 in the Mackenzie Delta, comprising nearly half of the total. These lagoons are also the smallest on average, at 2.0 km<sup>2</sup>. In contrast, lagoons along the coast of the Chukchi Sea present the largest average size at 23.9 km<sup>2</sup>. The coast of the East Siberian Sea shows the lowest density of thermokarst lagoons. Most lagoons along the Laptev Sea coast are located in the Lena Delta (87).

In summary, there are 152 lagoons in delta regions, accounting for 29% of the total lagoons, occupying 78% of the total lagoon area. Lagoons in delta environments are larger on average (17.8 km<sup>2</sup>) compared to lagoons outside of delta environments (2.0 km<sup>2</sup>). In contrast, most lagoons (69%) are part of a lagoon system and account for 80% of the total lagoon area. Single lagoons (see example in Figure 3) along straight coastlines are fewer and smaller on average (4.2 km<sup>2</sup>) compared to lagoons in lagoon systems (7.7 km<sup>2</sup>).

Additionally, the classification of lagoons into different connectivity classes further highlights variations in distribution. More than half (55%) are very low and low connected lagoons (Classes 1 and 2). Highly connected lagoons (Class 4) have the largest average area of 11.1 km<sup>2</sup>. Very highly connected Class 5 lagoons are the fewest and smallest (on average 4.6 km<sup>2</sup>).

We extracted the length of the coastlines from the pan-Arctic catchment database (ARCADE) and calculated the average lagoon and lake density per 100 km coastline length, which was highest for the Canadian Beaufort Sea with 8.3 lagoons and 51.0

lakes per 100 km, followed by the Alaskan Beaufort Sea (2.6 and 35.8). Lagoon and lake density were similar for the Chukchi Sea (1.2 and 17.9) and Laptev Sea with (1.3 and 17.0). The East Siberian Sea has the lowest lagoon density (0.9) but a higher lake density (22.6) than Chukchi and Laptev seas.

### 3.2 | Lagoon Area Change

Here, we present the results of the lagoon area change analysis from 2000 to 2021. The data were aggregated by region, class, and lagoon type to identify similarities and variations in lagoon connection. The most intense lagoon shrinking and growing was observed for two single Class 1 and Class 2 lagoons located at the Alaska Beaufort Sea (Table 3).

#### 3.2.1 | Regional Changes

The analysis of thermokarst lagoon area changes revealed growth across all five regions (Table 3) with significant differences ( $p < 0.05$ ) in lagoon area trends (Figure S4). Specifically, the lagoon area change at the Laptev Sea differed significantly from the East Siberian, Chukchi and Alaska Beaufort seas, whereas the Canadian Beaufort Sea also showed distinct trends compared to these three regions.

The strong change was observed for the Alaska Beaufort Sea, with a growth of 1.34%, followed by the East Siberian Sea at

**TABLE 3** | Lagoon area change for various Arctic regions and categories including maximum negative (shrinking) and positive (growing) area changes. Mean change represents the average percentage change for individual lagoons, with a standard deviation (SD) indicating variability. Overall change reflects the total change within each region, type or class.

Category		Initial lagoon area (km <sup>2</sup> )	Absolute change (km <sup>2</sup> )	Maximum negative change (km <sup>2</sup> )	Maximum positive change (km <sup>2</sup> )	Mean change (%)	SD of change (%)	Overall change (%)
Region	Canadian Beaufort Sea	584.4	2.9	-0.04	0.05	0.75	0.97	0.49
	Alaska Beaufort Sea	227.0	3.0	-0.28	0.14	1.23	5.49	1.34
	Chukchi Sea	563.8	4.7	-0.01	0.05	1.16	1.09	0.84
	East Siberian Sea	135.7	1.5	-0.19	0.13	1.91	4.65	1.08
	Laptev Sea	522.4	5.2	-0.04	0.09	0.68	2.02	1.00
	Lena Delta	421.0	1.7	-0.04	0.04	0.15	1.39	0.39
Type	Mackenzie Delta	205.6	0.4	-0.04	0.03	0.54	0.94	0.19
	Non-delta	1406.6	15.3	-0.28	0.14	1.19	3.08	1.09
	Single lagoon	510.6	7.6	-0.28	0.14	1.21	4.51	1.49
	Part of lagoon system	1522.6	9.7	-0.04	0.07	0.82	1.25	0.64
	Connectivity class	1	451.2	5.1	-0.18	0.14	1.38	2.73
	2	428.1	2.0	-0.28	0.1	0.45	4.09	0.47
	3	520.0	5.9	-0.04	0.06	0.87	1.48	1.14
	4	426.9	2.4	-0.01	0.13	0.96	1.71	0.56
	5	196.6	1.0	-0.01	0.03	0.65	0.66	0.50

1.08%, Laptev Sea at 1.00%, Chukchi Sea at 0.84% and Canadian Beaufort Sea, which experienced the lowest increase at 0.49%. The Wilcoxon signed-rank test revealed that the East Siberian, Chukchi and Alaska Beaufort seas showed significant deviations ( $p < 0.05$ ), whereas the Laptev and Canadian Beaufort seas were statistically similar to the entirety of lagoon change. The variance per region, represented by the standard deviation (SD), correlates directly with overall regional change, suggesting that regions with substantial increases also exhibit greater variability among lagoons.

In the category 'single lagoons', the highest average increase of  $1.91\% \pm 4.65\%$  was observed for lagoons located at the East Siberian Sea. However, due to their smaller size, these lagoons have a limited impact on the overall regional budget. In contrast, thermokarst lagoons in other regions exhibit mean change rates ranging from 0.68% to 1.23% (Table 3). Notably, lagoons along the Alaska Beaufort Sea and East Siberian Sea coasts display the greatest variability in area changes (Figure 5a).

Temporal variation in lagoon area shows a general increase over time, with short-term fluctuations of varying degrees (Figure 6). However, due to the inherent noise in the input data, making definitive assumptions about these fluctuations is challenging. Nonetheless, the long-term trend of area increase is clearly evident.

### 3.2.2 | Lagoon Change by Class

Among lagoon classes, Class 4 differed significantly from Classes 1 to 3, though these results were markedly weaker ( $p > 0.027$ ; Figure S5) than the regional comparisons ( $p > 1.8 \times 10^{-8}$ ). Analysis of individual lagoon classes revealed marginal significance for Class 1 ( $p = 0.037$ ) and Class 3 ( $p = 0.049$ ), whereas Class 4 was highly significant ( $p < 0.001$ ). Classes 1 and 3 demonstrate the strongest overall growth (Figure 5b), with increases of 1.13% and 1.14%, respectively (Table 3). However, individual lagoons within these classes show average growth rates of  $1.37\% \pm 2.73\%$  and  $0.87\% \pm 4.09\%$ , indicating that smaller lagoons are expanding more rapidly. Despite this, the expansion of smaller lagoons does not significantly affect the overall area change.

### 3.2.3 | Lagoon Changes in River Deltas

Non-deltaic lagoons exhibit stronger growth compared to lagoons within the Lena and Mackenzie Deltas (Figure 5c). Non-deltaic lagoons show an overall area increase of 1.09% and a mean increase of  $1.19\% \pm 3.08\%$  (Table 3). In contrast, lagoons in the deltas grew significantly slower, with an overall increase of 0.39% in the Lena Delta and 0.19% in the Mackenzie Delta. However, when looking at individual lagoons, those in the

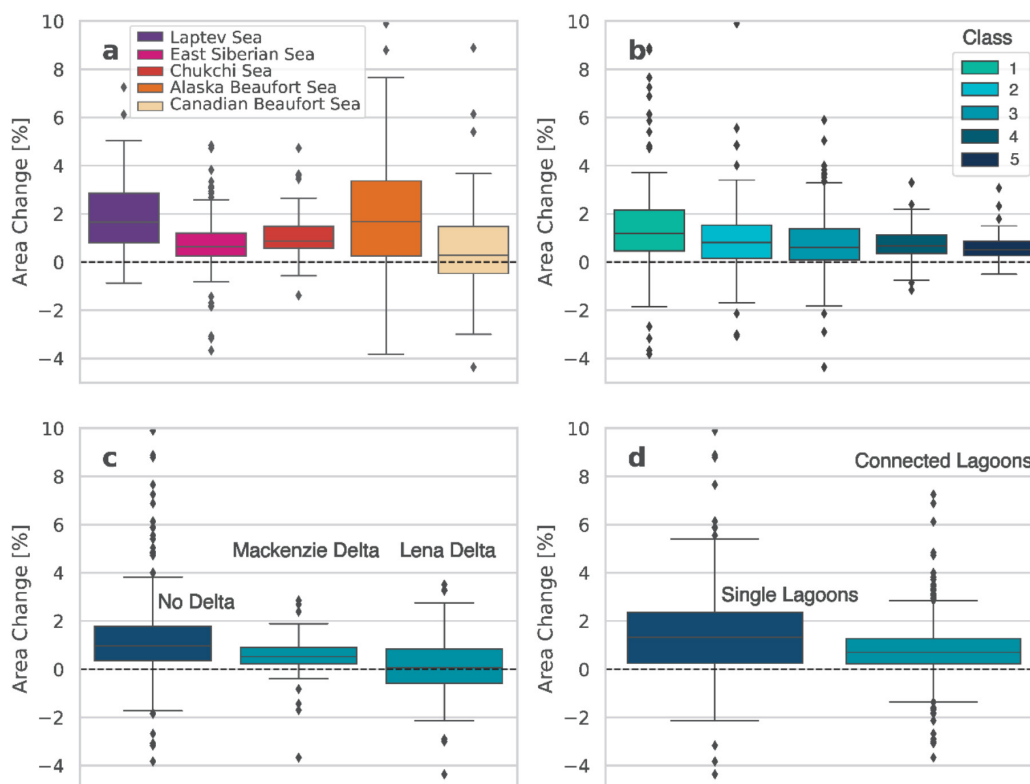


**FIGURE 5** | Boxplots of normalised lagoon area change trends (% change 2000–2021) per (a) region, (b) class, (c) delta and (d) lagoon system. [Colour figure can be viewed at [wileyonlinelibrary.com](https://onlinelibrary.wiley.com)]

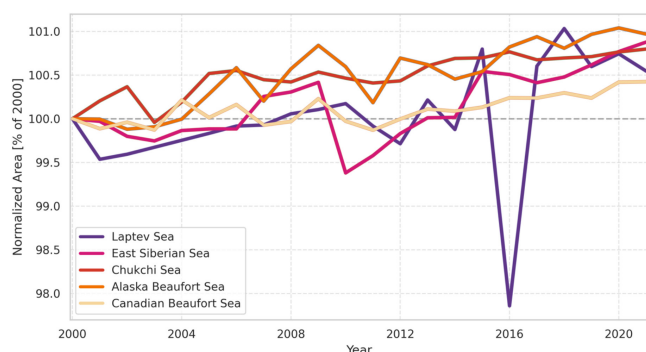


**FIGURE 6** | Annual lagoon area per region for the years 2000–2021, as area anomaly in % in reference to the base year 2000. [Colour figure can be viewed at [wileyonlinelibrary.com](https://onlinelibrary.wiley.com)]

Mackenzie Delta grew slightly faster but with less variability, on average, at  $0.54\% \pm 0.94\%$ , compared to the Lena Delta at  $0.15\% \pm 1.39\%$ . This suggests that non-deltaic lagoons are expanding faster, but there are also differences in the growth rates of individual lagoons between both delta regions.

### 3.2.4 | Changes in Connected Lagoon Systems

Lagoons that are part of larger connected systems exhibit weaker growth with less variability than non-connected lagoons (Figure 5d). The overall area of connected lagoons grew by 0.63% and, on average, by  $0.82\% \pm 1.25\%$  per individual lagoon

(Table 3). In contrast, the overall area of non-connected lagoons grew by 1.49% and, on average, by  $1.21\% \pm 4.51\%$  per individual lagoon, signifying the much stronger variation of non-connected lagoons.

### 3.2.5 | Individual Lagoon Examples

Most lagoons exhibit a slow growth over the observed period. Here, we highlight the case of lagoon ABS\_024 (Figure S6) on the Alaska Beaufort Sea coast at Cape Halkett, northeast of Teshekpuk Lake, which lost up to 36.1% of its area between 2012 and 2016, though it recovered to over 85% of the maximum area. The drainage of this particular water body was extensively covered by Jones and Arp [55] and will be discussed in the context of lagoon formation.

More detailed case studies can be found in the [Supporting Information](#), highlighting some thermokarst lagoons that deviate from the general trends, showing especially strong increase or decrease in water area.

## 3.3 | Comparison Between Thermokarst Lagoon and Lake Area

The comparison of lake and lagoon sizes across all study regions show revealed that both lakes and lagoons follow a strongly right-skewed size distribution, with the majority of features being relatively small (Figure S8). Although lakes are far more numerous than lagoons, the overall shape of the size distributions is very

similar, especially in the Canadian and Alaskan Beaufort seas. In total, 55% of lagoons are similar in size to nearby lakes, with a maximum deviation of 11%, and 95% differ by less than 5%. Many of them are located along the Beaufort Sea coast (Figure S9). Additionally, 40% show moderate size differences of up to 21%, whereas only 5% exhibit large deviations ranging from 31% to 41%. Most lagoons are smaller than the surrounding coastal lakes, with the exception of the 'very large' size only in the category, where 'very large' lagoons tend to be mainly larger. This pattern is particularly prominent along the Beaufort Sea coast (Figure S9S8).

## 4 | Discussion

Our methodological study employed for calculating the distribution, classification and area estimation of thermokarst lagoons along the Arctic coast provides a comprehensive overview of these unique water bodies across the Arctic coastal regions. To the best of our knowledge, no similar approach concerning thermokarst lagoons has been undertaken. The approach presented by Fraley et al. [22] aligns largely with our classification. Four out of five Arctic lagoons examined in both studies were classified as Class 1 or 'intermittent connection', which both emphasise the temporary nature of their limited connection.

### 4.1 | Geographical Distribution of Thermokarst Lagoons

The geographical distribution of thermokarst lagoons shows strong regional variation, primarily shaped by the interplay of coastal erosion dynamics, the presence of thermokarst lakes and local geomorphological conditions. Lagoon densities are highest along the Beaufort Sea coast, a region characterised by extensive lake-rich lowlands and rapid coastal erosion—reaching up to 48.8 m per year in extreme events (2007–2008; [10]) and averaging around 1.15–1.12 m per year for the Alaska and Canadian Beaufort seas [56]. These high erosion rates, combined with widespread ground-ice and low-lying terrain, promote frequent inland migration of the coastline, increasing the likelihood of coastal lakes being breached by the sea and transformed into lagoons. In contrast, the Chukchi Sea region, with significantly lower erosion rates—averaging just 0.20–0.49 m per year [10, 56]—shows much lower lagoon density, suggesting that slower coastal retreat reduces the frequency of lagoon formation.

The distribution of lagoons also strongly correlates with areas of high lake thermokarst activity. Based on regional thermokarst coverage data [57], 90% of lagoons are found in areas where lake thermokarst affects 60%–100% of the landscape, whereas only 5% occur in regions with low thermokarst presence (1%–30%) (Figure S2). This highlights the critical role of pre-existing thermokarst lakes in enabling lagoon development. However, this relationship is not uniform across the Arctic. For example, the western East Siberian Sea coast, despite high lake thermokarst coverage, shows a surprisingly low density of lagoons. This could be caused by elevation differences between former lake basins and the sea, which, if larger than spring tide heights, inhibit effective flooding and thus prevent lagoon formation.

In addition to spatial patterns, size comparisons further support the close link between lakes and lagoons. Across all regions, both features exhibit strongly right-skewed size distributions dominated by small water bodies (Figure S7). This similarity indicates that lagoon size is closely tied to the size of the original lakes, with most lagoons being slightly smaller than nearby lakes. The exception is the 'very large' category, where lagoons often exceed lake sizes (Figure S8)—potentially due to local geomorphic processes or post-formation changes such as the connection of neighbouring lagoon and the formation of larger lagoon systems. These patterns suggest that lagoon formation is primarily controlled by the distribution and size of thermokarst lakes, whereas coastal erosion modulates the timing and frequency of their transformation into lagoons.

We connected the mapped thermokarst lagoons with ground ice and organic carbon content data from the Arctic Coastal Database [58]. The findings reveal that 38% of all mapped thermokarst lagoons are located in areas with low ground ice content (0%–20%). The majority—about 53%—are found in regions with medium ground ice content (21%–50%). Only 9% of thermokarst lagoons are situated in areas with high ground ice content (> 50%), primarily located along the Alaska Beaufort Sea and the US Chukchi Sea.

Additionally, nearly 80% of the lagoons are located in areas where the organic carbon content is low (0%–2%) to medium (2%–5%). At thermokarst-affected coasts, permafrost thaw has already advanced significantly, and the stored organic matter has been decomposed over a long period. Furthermore, mixing with mineral-rich, OC-poor marine sediments could lead to a reduction in OC content in thermokarst lagoon sediments. However, field data suggest high variability in OC content between lagoons [28, 30, 45] (Jenrich et al. unpublished data). Young, less connected lagoons tend to retain terrestrial OC-rich sediment for longer periods, whereas more open lagoons experience faster sediment export due to stronger currents transporting material into the open ocean. About 21% of thermokarst lagoons are located in regions with high OC content (> 5%). In these lagoons, present mostly along the coasts of the Beaufort and Chukchi seas, the potential for elevated greenhouse gas (GHG) production is particularly high.

#### 4.1.1 | Regional Distribution of Lagoon Classes

Our classification of lagoons based on connectivity revealed important trends. More than half of the lagoons (55%) were classified as nearly closed (Class 1) and limited open (Class 2), indicating very low connectivity. These lagoons are critical in understanding the initial stages of the lake-to-sea transition and their potential for organic carbon degradation. Highly connected lagoons (Class 4) had the largest average area (11.1 km<sup>2</sup>), highlighting the advanced stages of the transition process. Interestingly, Class 5 lagoons, representing the most advanced stage, were the fewest and smallest (average 4.6 km<sup>2</sup>), suggesting that as lagoons become more connected to the sea, their overall area may decrease due to factors such as increased erosion and sediment redistribution.

When normalised to account for the total number of lagoons in each region, the distribution of lower-connected lagoons (Classes 1–3) appears more consistent across different regions (Figure S1a–c). In contrast, the more open and highly connected lagoons (Classes 4 and 5) are primarily concentrated in deltas and areas with high thermokarst activity, particularly along the Beaufort Sea and Laptev Sea coasts (Figure S1d,e). In these lowland regions, which are highly shaped by thermokarst processes, the combination of surface subsidence, sea-level rise and elevated erosion rates are drivers for the rapid drowning of thermokarst lakes [25]. This process results in large lagoon systems (Figure 3), which account for more than two-thirds of the mapped lagoons and take up 80% of the total lagoon area.

These patterns highlight the interplay between geomorphological setting, lagoon connectivity and sediment composition, underscoring the potential for substantial spatial variability in carbon cycling and GHG emissions across Arctic thermokarst lagoons.

## 4.2 | Patterns of Thermokarst Lagoon Area Change

As thermokarst lagoon area is likely closely linked to coastal erosion rates, patterns of thermokarst lagoon area change might correlate with those of Arctic coastal erosion rates. Along the Alaskan Beaufort Sea coast, coastal erosion rates are especially high [10]. The high variability and strong growth found in the thermokarst lagoons of this region may be especially influenced by coastal erosion. In contrast, the East Siberian Sea, Chukchi Sea and Laptev Sea generally exhibit slightly lower area growth. The stability of thermokarst lagoons along the Canadian Beaufort Sea stands in contrast to the erosivity along this coast. The overall trend of coastal erosion rather than progradation does not explain the observed stability, which may be coupled to other environmental factors. Importantly, many of these lagoons are part of larger lagoon systems, which can mitigate the expected impacts of coastal erosion due to reduced wave energy in these more sheltered environments. Overall, the analysis of the influence of coastal erosion would benefit greatly from a more in-depth quantitative assessment, which could be conducted with the help of the presented dataset.

At class level, the lack of a clear trend of change rates based on connectivity may be due to the highly variable distribution of lagoon classes along Arctic coasts, especially for Classes 1–3. Meanwhile, the location of many Class 4 and 5 lagoons in delta environments could point towards lower change in these delta environments. Nevertheless, the argument of subjectivity with classification based on geomorphology is one that should not be ignored and may have a slight influence on the lack of a clear trend. The inherent complexity of thermokarst lagoons indicates that although they can be classified based on their connectivity to the sea, each lagoon may still display different characteristics such as sediment grain size, shoreline elevation or ground ice content of the surrounding permafrost, which influences area changes. The implication here is that river delta and lagoon system environments are more influential on lagoon area change than classification.

Lagoons within systems may experience less change due to reduced wave energy, as the interconnected lagoons act as natural buffers. In particular, subsequent lagoons in these systems are shielded from wave action by the preceding ones, functioning like natural breakwaters. This is comparable to how Tuktoyaktuk Island, though actively eroding, serves as a protective barrier for the coastal Hamlet of Tuktoyaktuk located further inland on the Tuktoyaktuk Peninsula [59]. Exemplary own field observations during a very stormy boat ride from Reindeer Island (located near the outer Mackenzie Delta) back to Inuvik after finishing field work revealed very low wave activity in this specific lagoon system. These observations from 2021 are supported by Hill and Solomon [60], who report low wave frequency in the system, with the presence of aeolian deposits on lagoon shorelines indicating low erosional energy.

Overall, Arctic wave energy is projected to increase [61], driven by factors such as a longer open-water season [62] and higher storm intensity [63]. This raises the question of how thermokarst lagoons will be affected. Malito et al. [61] modelled wave energy along the Alaskan Beaufort Sea, finding that shelf geometry plays a crucial role—the steeper the shelf, the higher the wave energy reaching the coast. Generally, the shelves of the Beaufort, Chukchi, Laptev and East Siberian seas are characterised by low relief [64] and tend to be less impacted by high wave energy [61]. Previous studies at Reindeer Island and Bykovsky Peninsula (Laptev Sea) have shown that the depth of Class 3 to Class 5 lagoons ranges from 2 to 2.5 m [21, 28]. These shallow lagoons, combined with low-relief shelves, may be less vulnerable to coastal erosion from breaking waves than steeper or more exposed coastlines. Although this may not represent all pan-Arctic lagoons, we hypothesise that, although wave energy is an important factor, it may play a lesser role in lagoon growth compared to other drivers—particularly thermal erosion, which occurs on a much larger scale along permafrost coasts [61, 63].

Climate change-induced sea-level rise could drive lagoon growth and formation. Although this rise occurs at a rate of only millimetres per year [61], rising sea levels in Arctic lowlands—combined with factors such as increased storm intensity [63]—could flood coastal thermokarst lakes if the elevation difference between the lake and the sea is small enough. Over time, thermokarst lagoons may progress through different connectivity stages, from Class 1 to Class 5, creating a complex, evolving shoreline. These lagoons are gradually eroded over long timescales, eventually contributing to shoreline smoothing [27]. These lagoons are gradually eroded over long timescales, eventually contributing to shoreline smoothing. The potentially cyclical nature of thermokarst lagoons, along with the influence of sea-level rise, remains understudied, highlighting an important field for future research.

Individual lagoons that exhibit exceptional area changes may be influenced by local environmental processes and are not necessarily connected to global trends. However, lagoons such as ABS\_024 (Figure S7), which formed after a major lake drainage event in July 2014 [55], may represent the earliest stage in the lake-to-lagoon transition.

When drainage channels form due to the thermo-erosion of ice wedges [65, 66], thermokarst lakes can drain into the sea,

causing water levels to equalise with sea level. These connecting channels are commonly observed in many Class 1 and Class 2 lagoons (e.g., *Polar Fox Lagoon SLS\_003* and other lagoons listed in Table 1) and may have formed through thermo-erosion [67]. Further thermo-erosion could potentially widen these channels, though this process has not yet been studied specifically in the context of thermokarst lagoons.

Coastal erosion can also erode the barrier between the lakes or drained lake basins and the sea—particularly in lowland areas [68, 69]. This appears to be the case for *ABS\_024*, where surrounding elevations are less than 1 m, according to ArcticDEM data [41]. As erosion breaches the barrier, a connection to the sea is established, allowing seawater intrusion.

As reported, *ABS\_024* expanded its surface area to nearly match its pre-drainage maximum lake size, likely driven by enhanced seawater inflow. We propose that *ABS\_024* serves as a prime example of an early-stage thermokarst lagoon formation.

### 4.3 | Implications

Even though the majority of thermokarst lagoons are located in areas where the organic carbon content is low, most (55%) of the mapped thermokarst lagoons are young, less connected

lagoons (Classes 1 and 2), which may have higher GHG emissions (Figure 7). Incubation and microbiology studies have revealed that under the occurring brackish conditions, methane production is highest in these first stages of land-sea transition [2, 32, 70]. More connected thermokarst lagoons (3, 4) gradually receive more seawater and experience more sediment exchange with the sea, causing a decrease in organic matter availability and a shift towards marine microbial communities [2]. In this course,  $\text{CH}_4$  production decreases drastically. Fully connected, open lagoons (5) show more marine characteristics. GHG production shifts from a  $\text{CH}_4$  ratio of 1:1 in low connected lagoons to pure  $\text{CO}_2$  production (Figure 7 [2, 45]).

Our comprehensive dataset provides a robust foundation for future research on the biogeochemical processes within Arctic thermokarst lagoons. The detailed classification and area calculations provide a basis for extrapolation of more detailed local studies and enable more precise assessments of organic carbon degradation and nitrogen cycling—both of which are critical for understanding the broader implications of permafrost thaw at the land-ocean frontier with climate change. Beyond openness, local factors—particularly freshwater [71, 72], sediment [73–75] and organic matter inputs [76–78] in deltaic and estuarine environments—shape the hydrochemistry and biogeochemical properties of these lagoons, highlighting their variability and complexity.

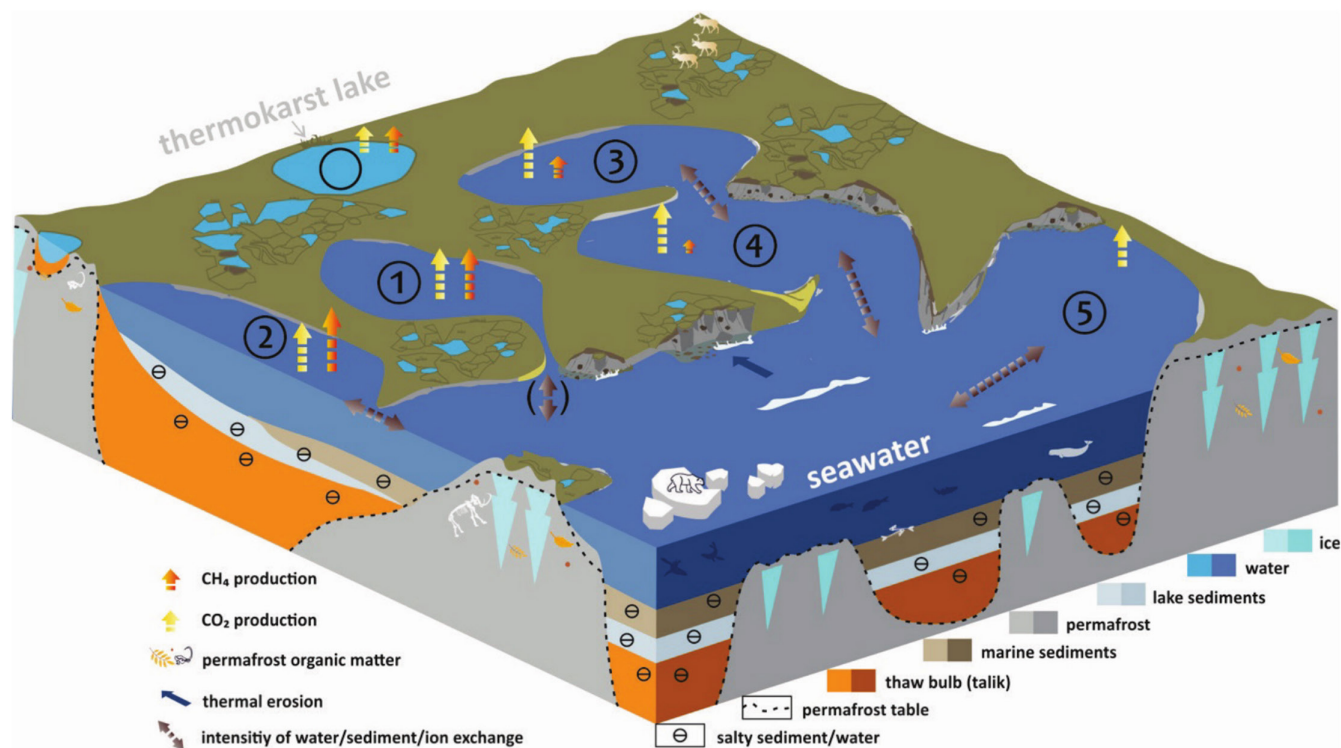


**FIGURE 7** | Schematic representation of the transformation of thermokarst lakes into lagoons and their progression towards fully marine systems due to permafrost thaw and coastal erosion in the Arctic. The diagram illustrates different stages of lagoon connectivity with the sea (1–5), highlighting methane ( $\text{CH}_4$ ) and carbon dioxide ( $\text{CO}_2$ ) production (red and yellow arrows) as a result of the breakdown of permafrost organic matter. Younger, less connected lagoons show higher  $\text{CH}_4$  production, while more marine-influenced systems have increased  $\text{CO}_2$  production. Subsurface features such as thaw bulbs (talik) and the permafrost table are depicted, along with sediment, water and ion exchange processes (black-grey arrows). The ongoing thermal erosion and seawater intrusion contribute to the thawing of permafrost and the migration of Arctic coastlines. This process may result in increased greenhouse gas emissions from Arctic coastal systems. Figure modified after Romanovskii et al. [20], information on  $\text{CO}_2$  and  $\text{CH}_4$  production rates is based on Jenrich et al. [2] and Jenrich et al. [45]. [Colour figure can be viewed at [wileyonlinelibrary.com](https://onlinelibrary.wiley.com)]

There is also progress in other related fields covering Arctic land-to-sea frontier environments, such as studies assessing the specific ecology of Arctic lagoons [13, 33, 79], the carbon and nitrogen pools of Arctic delta deposits (Fuchs et al., submitted) [80] or modelling the morphodynamics of Arctic river deltas where many thermokarst lagoons were found [81, 82].

Whereas our analysis provides insight into the modern (~20-year) variability of lagoon area, the extent to which these changes fall within long-term natural variability remains uncertain. Over longer timescales, Holocene climate fluctuations and postglacial transgression have likely influenced lagoon formation and change rates [20, 27], potentially leading to different patterns of variability compared to today. Future research incorporating palaeoenvironmental reconstructions and sea-level change modelling could help determine whether the observed trends align with past lagoon evolution or if recent changes reflect a shift beyond natural variability.

Further research should focus actual rates of transition from thermokarst lake to lagoon and the associated environmental impacts. A special focus should be placed on thermokarst lagoon systems, as they cover large areas with likely a high portion of organic carbon and nitrogen included [7] but have been scarcely studied so far. Additionally, expanding the analysis to include the Kara and Barents Sea coasts can help identify broader patterns and regional differences, enhancing our understanding of these dynamic ecosystems.

## 5 | Conclusion

This study provides the first comprehensive pan-Arctic assessment of thermokarst lagoons, including an updated analysis of their distribution and size, the introduction of a new classification approach and the first 20-year lagoon area change analysis. Our refined mapping revealed a detailed dataset of lagoon distribution and size, uncovering significant regional patterns in lagoon density—highest along the Beaufort Sea coast and lower across the Laptev, Chukchi and East Siberian Sea coasts.

Categorising thermokarst lagoons by their degree of openness provides new insights into the evolution of these dynamic coastal systems. This framework supports future research on how biogeochemical, hydrochemical, and ecological processes change throughout the permafrost land-to-sea transition. Beyond openness, local factors—particularly freshwater, sediment and organic matter inputs in deltaic and estuarine environments—shape the hydrochemistry and biogeochemical properties of these lagoons, highlighting their variability and complexity.

Our time-series analysis of annual surface water area reveals both overall lagoon area expansion and marked regional differences. The greatest variability emerged along the Alaskan Beaufort Sea and East Siberian Sea coasts. Local processes like drainage events and thermal erosion appear to drive rapid changes. Coastal erosion, intensified by longer ice-free seasons, increasing sea water temperatures and increased storm intensity, is hypothesised to be a key driver of lagoon formation, whereas rising sea levels may further amplify the creation of new lagoons in Arctic lowlands.

At a broader scale, this study highlights how Arctic climate change is reshaping the Arctic coastline, fostering the formation of thermokarst lagoons and therefore potentially altering local hydrology and impacting ecosystems. These lagoons serve as critical transition zones between terrestrial and marine environments, playing a unique role in permafrost carbon cycling. Notably, 55% of the mapped lagoons are young and low-connected lagoons, where OC-rich terrestrial sediments get trapped longer compared to more open, connected lagoons, resulting in a high potential for increased GHG production in the first stages of land-to-sea transition. Understanding the distribution and evolution of thermokarst lagoons is essential for predicting future landscape transformations and their global climate implications, making this research a crucial step towards better understanding the Arctic's response to climate change.

## Acknowledgements

Ideas for this research were initially developed in the German Federal Ministry of Education and Research (BMBF) research projects KoPF (Carbon in Permafrost; #03F0764B), KoPF-Synthesis (03F 0834B) and CACOON (Changing Arctic Carbon cycle in the Coastal Ocean Near-shore; #03F0806A). We thank Sebastian Laboor for helping to improve Figure 4. Open Access funding enabled and organized by Projekt DEAL.

## Conflicts of Interest

The authors declare no conflicts of interest.

## Data Availability Statement

All data generated in this study are available on the PANGAEA data repository: <https://doi.org/10.1594/PANGAEA.968886>.

## References

1. M. Fritz, J. E. Vonk, and H. Lantuit, "Collapsing Arctic Coastlines," *Nature Climate Change* 7 (2017): 6–7, <https://doi.org/10.1038/nclim.ate3188>.
2. M. Jenrich, M. Angelopoulos, S. Liebner, et al., "Greenhouse Gas Production and Microbial Response During the Transition From Terrestrial Permafrost to a Marine Environment," *Permafrost and Periglacial Processes* 36 (2024a): 63–82, <https://doi.org/10.1002/ppp.2251>.
3. D. M. Nielsen, P. Pieper, A. Barkhordarian, et al., "Increase in Arctic Coastal Erosion and Its Sensitivity to Warming in the Twenty-First Century," *Nature Climate Change* 12 (2022): 263–270, <https://doi.org/10.1038/s41558-022-01281-0>.
4. J. E. Vonk, L. Sánchez-García, B. E. van Dongen, et al., "Activation of Old Carbon by Erosion of Coastal and Subsea Permafrost in Arctic Siberia," *Nature* 489 (2012): 137–140, <https://doi.org/10.1038/nature11392>.
5. G. Hugelius, J. Strauss, S. Zubrzycki, et al., "Estimated Stocks of Circumpolar Permafrost Carbon With Quantified Uncertainty Ranges and Identified Data Gaps," *Biogeosciences* 11 (2014): 6573–6593.
6. U. Mishra, G. Hugelius, E. Shelef, et al., "Spatial Heterogeneity and Environmental Predictors of Permafrost Region Soil Organic Carbon Stocks," *Science Advances* 7 (2021): eaaz5236, <https://doi.org/10.1126/sciadv.aaz5236>.
7. J. Strauss, M. Fuchs, G. Hugelius, et al., "Organic Matter Storage and Vulnerability in the Permafrost Domain," in *Encyclopedia of Quaternary Science*, Third ed., ed. S. Elias (Elsevier, 2025), 399–410, <https://doi.org/10.1016/B978-0-323-99931-1.00164-1>.

8. C. D. Koven, E. a. G. Schuur, C. Schädel, et al., "A Simplified, Data-Constrained Approach to Estimate the Permafrost Carbon–Climate Feedback," *Philosophical Transactions of the Royal Society A: Mathematical, Physical and Engineering Sciences* 373 (2015): 20140423, <https://doi.org/10.1098/rsta.2014.0423>.
9. E. A. G. Schuur, B. W. Abbott, R. Commane, et al., "Permafrost and Climate Change: Carbon Cycle Feedbacks From the Warming Arctic," *Annual Review of Environment and Resources* 47 (2022): 343–371, <https://doi.org/10.1146/annurev-environ-012220-011847>.
10. A. M. Irrgang, M. Bendixen, L. M. Farquharson, et al., "Drivers, Dynamics and Impacts of Changing Arctic Coasts," *Nature Reviews Earth and Environment* 3 (2022): 39–54, <https://doi.org/10.1038/s43017-021-00232-1>.
11. J. Nitzbon, S. Westermann, M. Langer, et al., "Fast Response of Cold Ice-Rich Permafrost in Northeast Siberia to a Warming Climate," *Nature Communications* 11 (2020): 2201, <https://doi.org/10.1038/s41467-020-15725-8>.
12. P. C. Craig, "Fish Use of Coastal Waters of the Alaskan Beaufort Sea: A Review," *Transactions of the American Fisheries Society* 113 (1984): 265–282, [https://doi.org/10.1577/1548-8659\(1984\)113%3c265:FUOCWO%3e2.0.CO;2](https://doi.org/10.1577/1548-8659(1984)113%3c265:FUOCWO%3e2.0.CO;2).
13. K. H. Dunton, S. V. Schonberg, and L. W. Cooper, "Food Web Structure of the Alaskan Nearshore Shelf and Estuarine Lagoons of the Beaufort Sea," *Estuaries and Coasts* 35 (2012): 416–435, <https://doi.org/10.1007/s12237-012-9475-1>.
14. K. H. Dunton, T. Weingartner, and E. C. Carmack, "The Nearshore Western Beaufort Sea Ecosystem: Circulation and Importance of Terrestrial Carbon in Arctic Coastal Food Webs," *Progress in Oceanography* 71 (2006): 362–378, <https://doi.org/10.1016/j.pocean.2006.09.011>.
15. K. W. McMahon, W. G. Ambrose, M. J. Reynolds, B. J. Johnson, A. Whiting, and L. M. Clough, "Arctic Lagoon and Nearshore Food Webs: Relative Contributions of Terrestrial Organic Matter, Phytoplankton, and Phytobenthos Vary With Consumer Foraging Dynamics," *Estuarine, Coastal and Shelf Science* 257 (2021): 107388, <https://doi.org/10.1016/j.ecss.2021.107388>.
16. K. H. Dunton, T. Whiteaker, and B. McMeans, "LTER: Seasonal Controls and Emergent Effects of Changing Land-Ice-Ocean Interactions on Arctic Coastal Ecosystems (BLE II) (Project Proposal)," University of Texas at Austin, (2023).
17. LTER Core Research Areas, "LTER," (2019), accessed September 19, 2024, <https://lternet.edu/core-research-areas/>.
18. A. E. Stanek, V. R. von Biela, S. M. Laske, R. L. Taylor, and K. H. Dunton, "Barrier Islands Influence the Assimilation of Terrestrial Energy in Nearshore Fishes," *Estuarine, Coastal and Shelf Science* 278 (2022): 108094, <https://doi.org/10.1016/j.ecss.2022.108094>.
19. S. E. Grasby, I. Rod Smith, T. Bell, and D. L. Forbes, "Cryogenic Formation of Brine and Sedimentary Mirabilite in Submergent Coastal Lake Basins, Canadian Arctic," *Geochimica et Cosmochimica Acta* 110 (2013): 13–28, <https://doi.org/10.1016/j.gca.2013.02.014>.
20. N. N. Romanovskii, H.-W. Hubberten, A. V. Gavrilov, et al., "Thermokarst and Land–Ocean Interactions, Laptev Sea Region, Russia," *Permafrost and Periglacial Processes* 11 (2000): 137–152, [https://doi.org/10.1002/1099-1530\(200004/06\)11:2%3c137::AID-PPP345%3e3.0.CO;2-L](https://doi.org/10.1002/1099-1530(200004/06)11:2%3c137::AID-PPP345%3e3.0.CO;2-L).
21. S. Solomon, P. J. Mudie, R. Cranston, T. Hamilton, S. A. Thibaudeau, and E. S. Collins, "Characterisation of Marine and Lacustrine Sediments in a Drowned Thermokarst Embayment, Richards Island, Beaufort Sea, Canada," *International Journal of Earth Sciences* 89 (2000): 503–521, <https://doi.org/10.1007/s005310000126>.
22. K. M. Fraley, T. Jones, M. D. Robards, B. Smith, M. Tibbles, and A. Whiting, "The Forgotten Coast: A Synthesis of Current Knowledge of Southern Chukchi Sea Lagoon Ecosystems," *Arctic* 75 (2022): 300–319, <https://doi.org/10.14430/arctic75608>.
23. M. Angelopoulos, P. P. Overduin, M. Jenrich, et al., "Onshore Thermokarst Primes Subsea Permafrost Degradation," *Geophysical Research Letters* 48 (2021): e2021GL093881, <https://doi.org/10.1029/2021GL093881>.
24. M. Jenrich, "Thermokarst Lagoons - Carbon Pools and Panarctic Distribution" (master's thesis, Alfred Wegener Institute, University of Potsdam, 2020), 1–69.
25. R. Creel, J. Guimond, B. M. Jones, et al., "Permafrost Thaw Subsidence, Sea-Level Rise, and Erosion Are Transforming Alaska's Arctic Coastal Zone," *Proceedings of the National Academy of Sciences* 121 (2024): e2409411121, <https://doi.org/10.1073/pnas.2409411121>.
26. A. Héquette, M.-H. Ruz, and P. R. Hill, "The Effects of the Holocene Sea Level Rise on the Evolution of the Southeastern Coast of the Canadian Beaufort Sea," *Journal of Coastal Research* 11, no. 2 (1995): 494–507.
27. M.-H. Ruz, A. Héquette, and P. R. Hill, "A Model of Coastal Evolution in a Transgressed Thermokarst Topography, Canadian Beaufort Sea," *Marine Geology* 106 (1992): 251–278, [https://doi.org/10.1016/0025-3227\(92\)90133-3](https://doi.org/10.1016/0025-3227(92)90133-3).
28. L. Schirrmeister, M. N. Grigoriev, J. Strauss, et al., "Sediment Characteristics of a Thermokarst Lagoon in the Northeastern Siberian Arctic (Ivashkina Lagoon, Bykovsky Peninsula)," *arktos* 4 (2018): 1–16, <https://doi.org/10.1007/s41063-018-0049-8>.
29. V. G. Cheverev, I. Y. Vidyapin, and V. E. Tumskoy, "Composition and Characteristics of the Thermokarst Lagoon Deposits, Bykovsky Peninsula" [in Russian], *Kriosfera Zemli* 11, no. 3 (2007): 44–50.
30. M. Jenrich, M. Angelopoulos, G. Grosse, et al., "Thermokarst Lagoons: A Core-Based Assessment of Depositional Characteristics and an Estimate of Carbon Pools on the Bykovsky Peninsula," *Frontiers in Earth Science* 9 (2021a): 637899, <https://doi.org/10.3389/feart.2021.637899>.
31. F. P. Giest, M. Jenrich, G. Grosse, et al., "Organic Carbon, Mercury, and Sediment Characteristics Along a Land–Shore Transect in Arctic Alaska," *Biogeosciences* 22 (2025): 2871–2887, <https://doi.org/10.5194/bg-22-2871-2025>.
32. S. Yang, S. E. Anthony, M. Jenrich, et al., "Microbial Methane Cycling in Sediments of Arctic Thermokarst Lagoons," *Global Change Biology* 29 (2023): 2714–2731, <https://doi.org/10.1111/gcb.16649>.
33. K. M. Fraley, M. D. Robards, M. C. Rogers, et al., "Freshwater Input and Ocean Connectivity Affect Habitats and Trophic Ecology of Fishes in Arctic Coastal Lagoons," *Polar Biology* 44 (2021): 1401–1414, <https://doi.org/10.1007/s00300-021-02895-4>.
34. M. Young, F. Feyrer, D. Fong, et al., "Ocean Connectivity Drives Trophic Support for Consumers in an Intermittently Closed Coastal Lagoon," *Estuarine, Coastal and Shelf Science* 264 (2022): 107665, <https://doi.org/10.1016/j.ecss.2021.107665>.
35. I. Spangenberg, P. P. Overduin, E. Damm, et al., "Methane Pathways in Winter Ice of a Thermokarst Lake–Lagoon–Coastal Water Transect in North Siberia," *Cryosphere* 15 (2021): 1607–1625, <https://doi.org/10.5194/tc-15-1607-2021>.
36. F. Günther, P. P. Overduin, I. A. Yakshina, T. Opel, A. V. Baranskaya, and M. N. Grigoriev, "Observing Muostakh Disappear: Permafrost Thaw Subsidence and Erosion of a Ground-Ice-Rich Island in Response to Arctic Summer Warming and Sea Ice Reduction," *Cryosphere* 9 (2015): 151–178, <https://doi.org/10.5194/tc-9-151-2015>.
37. A. M. Irrgang, H. Lantuit, G. K. Manson, F. Günther, G. Grosse, and P. P. Overduin, "Variability in Rates of Coastal Change Along the Yukon Coast, 1951 to 2015," *Journal of Geophysical Research. Earth Surface* 123 (2018): 779–800, <https://doi.org/10.1002/2017JF004326>.
38. B. M. Jones, A. M. Irrgang, L. M. Farquharson, et al., "Arctic Report Card 2020: Coastal Permafrost Erosion," (2020), <https://doi.org/10.25923/E47W-DW52>.

39. P. Marsh, M. Russell, S. Pohl, H. Haywood, and C. Onclin, "Changes in Thaw Lake Drainage in the Western Canadian Arctic From 1950 to 2000," *Hydrological Processes* 23 (2009): 145–158, <https://doi.org/10.1002/hyp.7179>.
40. I. Nitze, G. Grosse, B. Jones, et al., "Landsat-Based Trend Analysis of Lake Dynamics Across Northern Permafrost Regions," *Remote Sensing* 9 (2017): 640, <https://doi.org/10.3390/rs9070640>.
41. C. Porter, P. Morin, I. Howat, et al., "ArcticDEM, Version 3," (2018), <https://doi.org/10.7910/DVN/OHHUKH>.
42. "Copernicus Sentinel," (2024), Copernicus Data Space Ecosystem Browser.
43. M. Jenrich, M. Angelopoulos, P. P. Overduin, et al., "Distribution of Lagoons Along the Arctic Coast From the Taimyr Peninsula in Russia to the Tuktoyaktuk Peninsula in Canada," *PANGAEA* (2021b), <https://doi.org/10.1594/PANGAEA.934158>.
44. M. Jenrich, I. Nitze, S. Laboor, M. Angelopoulos, G. Grosse, and J. Strauss, "Spatial Extent of Thermokarst Lagoons Along Pan-Arctic Coasts - An Upscaling Approach," *PANGAEA* (2023), <https://doi.org/10.1594/PANGAEA.948267>.
45. M. Jenrich, M. Prodingler, I. Nitze, G. Grosse, and J. Strauss, "Pan-Arctic Thermokarst Lagoon Distribution, Area and Classification," *PANGAEA* (2024b), <https://doi.org/10.1594/PANGAEA.968886>.
46. J.-F. Pekel, A. Cottam, N. Gorelick, and A. S. Belward, "High-Resolution Mapping of Global Surface Water and Its Long-Term Changes," *Nature* 540 (2016): 418–422, <https://doi.org/10.1038/nature20584>.
47. N. Gorelick, M. Hancher, M. Dixon, S. Ilyushchenko, D. Thau, and R. Moore, "Google Earth Engine: Planetary-Scale Geospatial Analysis for Everyone," *Remote Sensing of Environment* 202 (2017): 18–27, <https://doi.org/10.1016/j.rse.2017.06.031>.
48. A. Beamish, M. K. Reynolds, H. Epstein, et al., "Recent Trends and Remaining Challenges for Optical Remote Sensing of Arctic Tundra Vegetation: A Review and Outlook," *Remote Sensing of Environment* 246 (2020): 111872, <https://doi.org/10.1016/j.rse.2020.111872>.
49. T. R. Loveland and J. R. Irons, "Landsat 8: The Plans, the Reality, and the Legacy," *Remote Sensing of Environment* 185 (2016): 1–6, <https://doi.org/10.1016/j.rse.2016.07.033>.
50. M. A. Wulder, T. R. Loveland, D. P. Roy, et al., "Current Status of Landsat Program, Science, and Applications," *Remote Sensing of Environment* 225 (2019): 127–147, <https://doi.org/10.1016/j.rse.2019.02.015>.
51. B. Lehner and P. Döll, "Development and Validation of a Global Database of Lakes, Reservoirs and Wetlands," *Journal of Hydrology* 296 (2004): 1–22, <https://doi.org/10.1016/j.jhydrol.2004.03.028>.
52. N. J. Speetjens, G. Hugelius, T. Gumbricht, et al., "The Pan-Arctic Catchment Database (ARCADE)," *Earth System Science Data* 15 (2023): 541–554, <https://doi.org/10.5194/essd-15-541-2023>.
53. J. Obu, S. Westermann, A. Bartsch, et al., "Northern Hemisphere Permafrost Map Based on TTOP Modelling for 2000–2016 at 1 km<sup>2</sup> Scale," *Earth Science Reviews* 193 (2019): 299–316, <https://doi.org/10.1016/j.earscirev.2019.04.023>.
54. Z. D. Tessler, C. J. Vörösmarty, M. Grossberg, et al., "Profiling Risk and Sustainability in Coastal Deltas of the World," *Science* 349, no. 6248 (2015): 638–643, <https://doi.org/10.1126/science.aab3574>.
55. B. M. Jones and C. D. Arp, "Observing a Catastrophic Thermokarst Lake Drainage in Northern Alaska," *Permafrost and Periglacial Processes* 26 (2015): 119–128, <https://doi.org/10.1002/ppp.1842>.
56. H. Lantuit, P. P. Overduin, N. Couture, et al., "The Arctic Coastal Dynamics Database: A New Classification Scheme and Statistics on Arctic Permafrost Coastlines," *Estuaries and Coasts* 35 (2012): 383–400, <https://doi.org/10.1007/s12237-010-9362-6>.
57. D. Olefeldt, S. Goswami, G. Grosse, et al., "Circumpolar Distribution and Carbon Storage of Thermokarst Landscapes," *Nature Communications* 7 (2016): 13043, <https://doi.org/10.1038/ncomms13043>.
58. H. Lantuit, P. P. Overduin, N. Couture, et al., "The ACD Classification of Arctic Coasts," (2020), <https://doi.org/10.1594/PANGAEA.919573>.
59. D. Whalen, D. L. Forbes, V. Kostylev, et al., "Mechanisms, Volumetric Assessment, and Prognosis for Rapid Coastal Erosion of Tuktoyaktuk Island, an Important Natural Barrier for the Harbour and Community," *Canadian Journal of Earth Sciences* 59 (2022): 945–960, <https://doi.org/10.1139/cjes-2021-0101>.
60. P. R. Hill and S. Solomon, "Geomorphologic and Sedimentary Evolution of a Transgressive Thermokarst Coast, Mackenzie Delta Region, Canadian Beaufort Sea," *Journal of Coastal Research* 15, no. 4 (1999).
61. J. Malito, E. Eidam, and J. Nienhuis, "Increasing Wave Energy Moves Arctic Continental Shelves Toward a New Future," *Journal of Geophysical Research: Oceans* 127 (2022): e2021JC018374, <https://doi.org/10.1029/2021JC018374>.
62. J. C. Stroeve, V. Kattsov, A. Barrett, et al., "Trends in Arctic Sea Ice Extent From CMIP5, CMIP3 and Observations," *Geophysical Research Letters* 39, no. 16 (2012): L16502, <https://doi.org/10.1029/2012GL052676>.
63. M. Lim, D. Whalen, J. Mann, et al., "Effective Monitoring of Permafrost Coast Erosion: Wide-Scale Storm Impacts on Outer Islands in the Mackenzie Delta Area," *Frontiers in Earth Science* 8 (2020), <https://doi.org/10.3389/feart.2020.561322>.
64. P. T. Harris, M. Macmillan-Lawler, J. Rupp, and E. K. Baker, "Geomorphology of the Oceans," *Marine Geology* 352 (2014): 4–24, <https://doi.org/10.1016/j.margeo.2014.01.011>.
65. D. Fortier, M. Allard, and Y. Shur, "Observation of Rapid Drainage System Development by Thermal Erosion of Ice Wedges on Bylot Island, Canadian Arctic Archipelago," *Permafrost and Periglacial Processes* 18 (2007): 229–243, <https://doi.org/10.1002/ppp.595>.
66. I. C. Nicu, H. Tanyas, L. Rubensdotter, and L. Lombardo, "A Glimpse Into the Northernmost Thermo-Erosion Gullies in Svalbard archipelago and Their Implications for Arctic Cultural Heritage," *Catena* 212 (2022): 106105, <https://doi.org/10.1016/j.catena.2022.106105>.
67. M. Angelopoulos, P. P. Overduin, S. Westermann, et al., "Thermokarst Lake to Lagoon Transitions in Eastern Siberia: Do Submerged Taliks Refreeze?," *Journal of Geophysical Research: Earth Surface* 125 (2020): e2019JF005424, <https://doi.org/10.1029/2019JF005424>.
68. K. M. Hinkel, B. M. Jones, W. R. Eisner, C. J. Cuomo, R. A. Beck, and R. Frohn, "Methods to Assess Natural and Anthropogenic Thaw Lake Drainage on the Western Arctic Coastal Plain of Northern Alaska," *Journal of Geophysical Research: Earth Surface* 112 (2007): 1–9, <https://doi.org/10.1029/2006JF000584>.
69. J. R. Mackay, "Catastrophic Lake Drainage, Tuktoyaktuk Peninsula Area, District of Mackenzie," *Geological Survey of Canada Paper* 88-1D (1988): 83–90.
70. M. Jenrich, J. Wolter, S. Liebner, et al., "Rising Arctic Seas and Thawing Permafrost: Uncovering the Carbon Cycle Impact in a Thermokarst Lagoon System in the Outer Mackenzie Delta, Canada," *Biogeosciences* 22 (2025): 2069–2086, <https://doi.org/10.5194/bg-22-2069-2025>.
71. C. M. Harris, J. W. McClelland, T. L. Connelly, B. C. Crump, and K. H. Dunton, "Salinity and Temperature Regimes in Eastern Alaskan Beaufort Sea Lagoons in Relation to Source Water Contributions," *Estuaries and Coasts* 40 (2017): 50–62, <https://doi.org/10.1007/s12237-016-0123-z>.
72. J. W. McClelland, R. M. Holmes, K. H. Dunton, and R. W. Macdonald, "The Arctic Ocean Estuary," *Estuaries and Coasts* 35 (2012): 353–368, <https://doi.org/10.1007/s12237-010-9357-3>.

73. S. Chalov, K. Prokopeva, D. Magritsky, et al., "Climate Change Impacts on Streamflow, Sediment Load and Carbon Fluxes in the Lena River Delta," *Ecological Indicators* 157 (2023): 111252, <https://doi.org/10.1016/j.ecolind.2023.111252>.
74. V. V. Gordeev, "Fluvial Sediment Flux to the Arctic Ocean," *Geomorphology, Sedimentary Source-to-Sink-Fluxes in Cold Environments* 80 (2006): 94–104, <https://doi.org/10.1016/j.geomorph.2005.09.008>.
75. J. E. Vonk Vonk, L. Giosan, J. Blusztajn, et al., "Spatial Variations in Geochemical Characteristics of the Modern Mackenzie Delta Sedimentary System," *Geochimica et Cosmochimica Acta* 171 (2015): 100–120, <https://doi.org/10.1016/j.gca.2015.08.005>.
76. J. Jung, Y. Lee, K.-H. Cho, E. J. Yang, and S.-H. Kang, "Spatial Distributions of Riverine and Marine Dissolved Organic Carbon in the Western Arctic Ocean: Results From the 2018 Korean Expedition," *Journal of Geophysical Research, Oceans* 127 (2022): e2021JC017718, <https://doi.org/10.1029/2021JC017718>.
77. S. E. Tank, M. Manizza, R. M. Holmes, J. W. McClelland, and B. J. Peterson, "The Processing and Impact of Dissolved Riverine Nitrogen in the Arctic Ocean," *Estuaries and Coasts* 35 (2012): 401–415, <https://doi.org/10.1007/s12237-011-9417-3>.
78. Y. Zhang, M. Yamamoto-Kawai, E. Watanabe, and H. Park, "How Much Can Riverine Biogeochemical Fluxes Affect the Arctic Ocean Acidification?," *Journal of Geophysical Research, Oceans* 129 (2024): e2023JC020404, <https://doi.org/10.1029/2023JC020404>.
79. S. M. Laske, V. R. von Biela, A. E. Stanek, and K. H. Dunton, "Local Environmental Conditions Structured Discrete Fish Assemblages in Arctic Lagoons," *Polar Biology* 47 (2024): 551–568, <https://doi.org/10.1007/s00300-024-03239-8>.
80. J. E. Vonk, A. F. Dickens, L. Giosan, et al., "Arctic Deltaic Lake Sediments as Recorders of Fluvial Organic Matter Deposition," *Frontiers in Earth Science* 4 (2016): 77, <https://doi.org/10.3389/feart.2016.00077>.
81. N.-H. Chan, M. Langer, B. Juhls, et al., "An Arctic Delta Reduced-Complexity Model and Its Reproduction of Key Geomorphological Structures," *Earth Surface Dynamics* 11 (2023): 259–285, <https://doi.org/10.5194/esurf-11-259-2023>.
82. A. Piliouras and J. C. Rowland, "Arctic River Delta Morphologic Variability and Implications for Riverine Fluxes to the Coast," *Journal of Geophysical Research - Earth Surface* 125 (2020): e2019JF005250, <https://doi.org/10.1029/2019JF005250>.

### Supporting Information

Additional supporting information can be found online in the Supporting Information section.